Hindawi Publishing Corporation
Mathematical Problems in Engineering
Volume 2012, Article ID 987256, 18 pages
doi:10.1155/2012/987256

Research Article

A Novel Dual-Loop Disturbance Observer-Based Attitude Control for a Space-Based Observation Microsatellite

Jian Sun, Jian Yu, and Haijun Rong

State Key Laboratory for Strength and Vibration of Mechanical Structures, School of Aerospace, Xi'an Jiaotong University, Xi'an 710049, China

Correspondence should be addressed to Haijun Rong, hjrong@mail.xjtu.edu.cn

Received 10 May 2012; Revised 28 June 2012; Accepted 29 June 2012

Academic Editor: Piermarco Cannarsa

Aiming at strong coupling and nonlinear dynamic equations for a space-based observation satellite, a sliding mode controller with feed-forward compensation is proposed in this paper. The theorem of moment of momentum is applied to formulate the exact nonlinear dynamic equations of a multibody satellite. On this basis, sliding-mode control-based, dual-loop forward-feed compensation control is used to control the attitude of the space-based observation microsatellite. By comparing with the conventional control method, simulation results demonstrate that the proposed control method has superior performance in terms of suppression from external disturbances and vibration. Better dynamic and static performance indices than the conventional control method are achieved.

1. Introduction

Space observation systems consist of two parts, that is, the space- and ground-based space observation systems. The latter is subject to atmospheric propagation jitter, astronomical refraction, ionosphere scintillation, and limits of national boundaries. Space-based observation techniques can effectively solve such problems and have the advantages of flexible maneuverability, wide monitoring ranges, long-distance observation, and so forth. Space-based observation is an important direction of future space target detection.

However, space-based observation satellites contain rotating rigid parts and flexible appendages. During the observation process, the rotation of rigid parts, elastic vibration of flexible appendages, and motion of satellite attitude influence each other, comprising

a strongly coupling nonlinear system. Highly accurate and highly stable attitude control is difficult to realize, especially for micro-satellites used in space target observation, because of the small mass and moment inertias of micro-satellites, as well as the limited quantity and capacity of actuators. Therefore, some special control methods should be applied to the attitude control system of space-based observation micro-satellites.

Numerous efforts have been exerted to achieve high-accuracy satellite attitude control. Cheng et al. [1] have used the feedback linearization method to eliminate the coupling terms between the attitude angular velocity and reaction wheel angular momentum, as well as reduce the influences of the vibration of panels and turning of rigid parts on the satellite attitude. Li et al. [2] have proposed a method combining variable structure control with neural networks based on the Lyapunov stability theory, which can ensure that the attitude angular velocity exponentially converges to the given limited range in the case of uncertain disturbance. Chen et al. [3] has proposed an adaptive mixed H_2/H_∞ attitude control for nonlinear spacecraft systems with unknown or uncertain inertia matrices and external disturbances. Experimental simulation results based on the Republic of China Satellite-1 spacecraft system are presented to demonstrate the effectiveness of the proposed design methods. Azadi et al. [4] have applied an adaptive-robust control scheme to control the three-axes maneuver of a flexible satellite. The controller is robust against disturbances and uncertainties, and adapted to the bounds of the unknown parameters of the system. Jan and Chiou [5] have applied sliding mode control to perform a rigid spacecraft large-angle maneuver in minimal time.

Modeling of nonlinear dynamic factors, parameter changes during movement, and external disturbances can be called disturbance terms. Disturbance observer (DOB) can suppress such disturbances. The design of observers has been investigated exhaustively in the theoretical framework and also in many related applications [6–10]. De La Sen and Luo [7] designs linear observers for a class of linear hybrid systems. Such systems are composed of continuous-time and digital substates and possess. Santhakumar [9] investigates the performance of a robust tracking control on the basis of proportional-derivative observer-based backstepping control applied on a three degrees of freedom underwater spatial manipulator. Yamashita et al. [6] have applied the disturbance observation-based PID control method to the Japanese satellite HALCA, whose mission is very long baseline interferometry observations in orbit.

However, all the above mentioned methods involve the linearization process or some simplification of the satellite dynamic model, which to some extent affects the final precision. In this paper, the nonlinear dynamic equations of multi-body satellites with flexible appendages and rigid turntables were explored based on the theorem of moment of momentum. On this basis, satellite attitude control with variable structure based on dual-loop feed-forward compensation of disturbance estimator was proposed. The mathematical simulation results showed that the proposed method is far superior to the traditional method of attitude control. The Lyapunov analysis and its treatment on stability and robustness of the proposed scheme under parameter uncertainties are not explicitly dealt with, and is left in this work for the scope of future work. The dynamic model of a space-based observation satellite derived in this paper has a high reference value for the design of attitude control systems of space-based observation satellites.

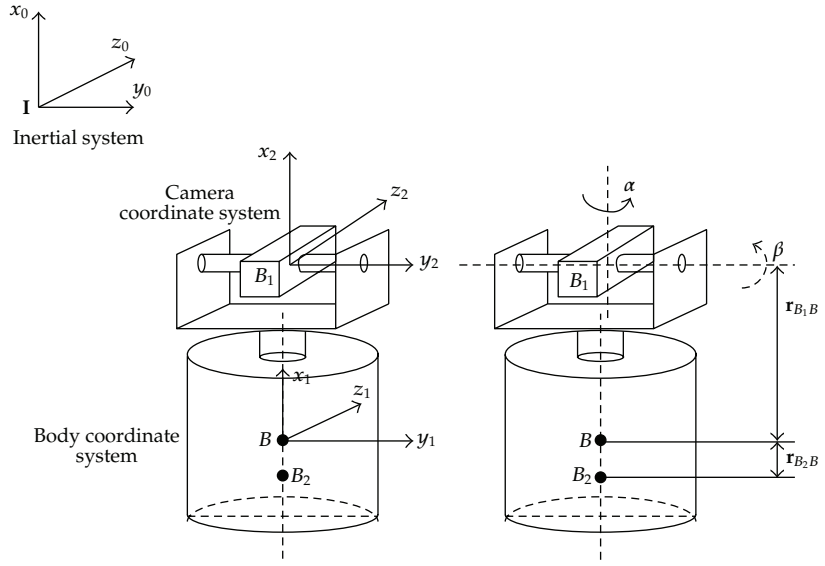

Figure 1: Simplified structure of a space-based observation satellite.

2. Dynamic Modeling of a Multi-Body Satellite

2.1. Kinematic Equation of a Space-Based Observation Satellite

The angular velocity of a camera coordinate system relevant to the satellite body frame is denoted as ω^{B_1B} so that its projection under a camera coordinate system is written as

$$\left[\boldsymbol{\omega}^{B_1B}\right]^{B_1} = \left[\omega_{x1} \quad \omega_{y1} \quad \omega_{z1}\right]^T. \tag{2.1}$$

As shown in Figure 1, the motion of the turntable of the camera along the z-axes is constrained relative to the satellite body. Therefore, the rotation angle turntable of the camera along the x_2- and y_2-axes in the camera coordination system is set as α and β. The corresponding angular velocities are $\dot{\alpha}$ and $\dot{\beta}$, respectively.

From Euler's theorem, the rotation of a rigid body around a fixed point can be decomposed into a number of limited rotations around such point. As shown in Figure 2, the coordinate transformation matrix $\mathbf{T}_{B_1B}$ from the satellite body coordinate system to the camera coordinate system with a rotation sequence of 2-3-1 is as follows:

$$\mathbf{T}_{B_1B}(\alpha,\beta,0) = \mathbf{T}_x(\alpha)\mathbf{T}_z(0)\mathbf{T}_y(\beta) = \begin{bmatrix} \mathrm{c}\beta & 0 & -\mathrm{s}\beta \\ \mathrm{s}\alpha\mathrm{s}\beta & \mathrm{c}\alpha & \mathrm{s}\alpha\mathrm{c}\beta \\ \mathrm{c}\alpha\mathrm{s}\beta & -\mathrm{s}\alpha & \mathrm{c}\alpha\mathrm{c}\beta \end{bmatrix}. \tag{2.2}$$

The angular velocity of the camera $\boldsymbol{\omega}^{B_1B}$ is connected to the transformation matrix $\mathbf{T}_{B_1B}$ by the following relationship:

$$\boldsymbol{\Omega}_{B_1B} = -\dot{\mathbf{T}}_{B_1B}(\alpha,\beta,0)\mathbf{T}^T_{B_1B}(\alpha,\beta,0), \tag{2.3}$$

where $\boldsymbol{\Omega}_{B_1B}$ is the antisymmetric matrix of $\boldsymbol{\omega}^{B_1B}$.

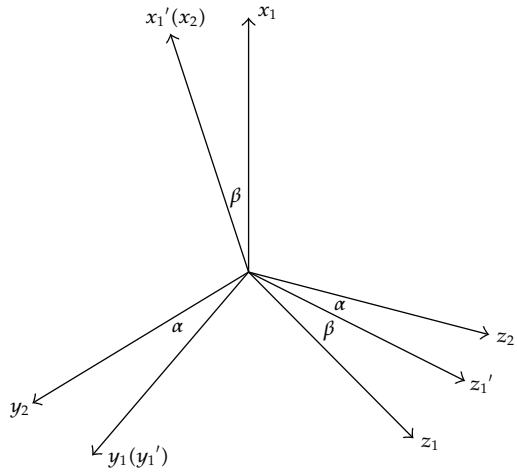

Figure 2: Transformation between the satellite body frame and camera frame.

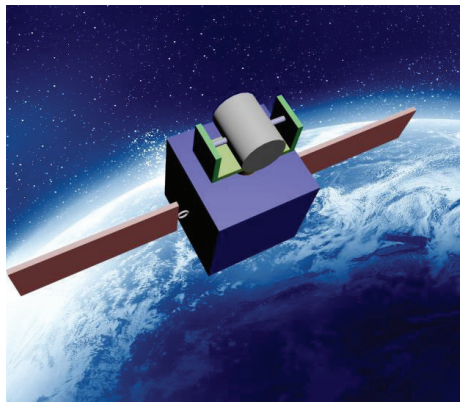

Figure 3: A space-based observation satellite.

Based on the above equation, the following matrix can be obtained:

$$\begin{bmatrix} \omega_{x1} \\ \omega_{y1} \\ \omega_{z1} \end{bmatrix} = \begin{bmatrix} \dot{\alpha} \\ c\alpha \cdot \dot{\beta} \\ -s\alpha \cdot \dot{\beta} \end{bmatrix}. \tag{2.4}$$

2.2. Dynamic Equations of a Space-Based Observation Satellite Attitude

As shown in Figure 3, a space-based observation satellite can be simplified into three parts: camera turntable, satellite body, and solar panels. The camera turntable and satellite body can be approximated as rigid bodies, and the solar panels as flexible appendages. The following subsections describe the attitude dynamic modeling of a space-based observation satellite.

2.2.1. Attitude Dynamic Modeling of a Space-Based Observation Satellite

A space-based observation satellite can be simplified into a camera turntable and a satellite body when not considering the reaction wheel and flexible appendages. In this case, the attitude dynamic equation can be derived from the theorem of moment of momentum as follows:

$$D^I \mathbf{L}_B^{BI} = \mathbf{M}_B, \tag{2.5}$$

where $\mathbf{L}_B^{BI}$ is the total moment of momentum, and $\mathbf{M}_B$ is the total outside torque the satellite experiences relative to the centroid B.

The total moment of momentum of satellite consists of two parts, which can be written as

$$\mathbf{L}_B^{BI} = \mathbf{L}_B^{B_1 I} + \mathbf{L}_B^{B_2 I}, \tag{2.6}$$

where $\mathbf{L}_B^{B_1 I}, \mathbf{L}_B^{B_2 I}$ can be expressed as

$$\begin{aligned} \mathbf{L}_B^{B_1 I} &= \mathbf{L}_{B_1}^{B_1 I} + m_{B_1} \mathbf{r}_{B_1 B} \times D^I \mathbf{r}_{B_1 B} = \mathbf{I}_{B_1}^{B_1} \boldsymbol{\omega}^{B_1 I} + m_{B_1} \mathbf{R}_{B_1 B} D^I \mathbf{r}_{B_1 B}, \\ \mathbf{L}_B^{B_2 I} &= \mathbf{I}_{B_2}^{B_2} \boldsymbol{\omega}^{B_2 I} + m_{B_2} \mathbf{R}_{B_2 B} D^I \mathbf{r}_{B_2 B}, \end{aligned} \tag{2.7}$$

where $\mathbf{R}_{B_1 B}$ represents the antisymmetric matrix of $\mathbf{r}_{B_1 B}$.

Equations (2.5)–(2.7) can yield

$$D^I \left(\mathbf{I}_{B_1}^{B_1} \boldsymbol{\omega}^{B_1 I} + m_{B_1} \mathbf{R}_{B_1 B} D^I \mathbf{r}_{B_1 B} + \mathbf{I}_{B_2}^{B_2} \boldsymbol{\omega}^{B_2 I} + m_{B_2} \mathbf{R}_{B_2 B} D^I \mathbf{r}_{B_2 B} \right) = M_B. \tag{2.8}$$

Given that $m_{B_1} \mathbf{r}_{B_1 B} + m_{B_2} \mathbf{r}_{B_2 B} = 0$, (2.8) can yield

$$D^I \left(\mathbf{I}_{B_1}^{B_1} \boldsymbol{\omega}^{B_1 I} \right) + D^I \left(\mathbf{I}_{B_2}^{B_2} \boldsymbol{\omega}^{B_2 I} \right) + D^I \left(m_{B_2} \mathbf{R}_{B_2 B} D^I \mathbf{r}_{B_2 B_1} \right) = M_B. \tag{2.9}$$

The transforms $D^I(\mathbf{I}_{B_1}^{B_1} \boldsymbol{\omega}^{B_1 I})$, $D^I(\mathbf{I}_{B_2}^{B_2} \boldsymbol{\omega}^{B_2 I})$, and $D^I(m_{B_2} \mathbf{R}_{B_2 B} D^I \mathbf{r}_{B_2 B_1})$ are discussed below.

For $D^I(\mathbf{I}_{B_1}^{B_1} \boldsymbol{\omega}^{B_1 I})$, based on the equation $D^I(s) = D^{B_1}(s) + \omega^{B_1 I} \times s$, we can obtain

$$D^I \left(\mathbf{I}_{B_1}^{B_1} \boldsymbol{\omega}^{B_1 I} \right) = D^{B_1} \left(\mathbf{I}_{B_1}^{B_1} \boldsymbol{\omega}^{B_1 I} \right) + \boldsymbol{\omega}^{B_1 I} \times \mathbf{I}_{B_1}^{B_1} \boldsymbol{\omega}^{B_1 I} = \mathbf{I}_{B_1}^{B_1} D^{B_1} \left(\boldsymbol{\omega}^{B_1 I} \right) + \boldsymbol{\Omega}^{B_1 I} \mathbf{I}_{B_1}^{B_1} \boldsymbol{\omega}^{B_1 I}, \tag{2.10}$$

where $\boldsymbol{\Omega}^{B_1 I}$ is the antisymmetric matrix of $\boldsymbol{\omega}^{B_1 I}$.

Given that $\omega^{B_1 I} = \omega^{B_1 B} + \omega^{BI}$, substitution into (2.10) yields

$$\begin{aligned} D^I \left(\mathbf{I}_{B_1}^{B_1} \boldsymbol{\omega}^{B_1 I} \right) = {} & \mathbf{I}_{B_1}^{B_1} D^{B_1} \boldsymbol{\omega}^{B_1 B} + \mathbf{I}_{B_1}^{B_1} D^B \boldsymbol{\omega}^{BI} + \left(\boldsymbol{\Omega}^{B_1 B} \mathbf{I}_{B_1}^{B_1} + \boldsymbol{\Omega}^{BI} \mathbf{I}_{B_1}^{B_1} - \mathbf{I}_{B_1}^{B_1} \boldsymbol{\Omega}^{B_1 B} \right) \boldsymbol{\omega}^{BI} \\ & + \left(\boldsymbol{\Omega}^{B_1 B} + \boldsymbol{\Omega}^{BI} \right) \mathbf{I}_{B_1}^{B_1} \omega^{B_1 B}. \end{aligned} \tag{2.11}$$

For $D^I(\mathbf{I}_{B_2}^{B_2}\boldsymbol{\omega}^{B_2I})$,

$$D^I\left(\mathbf{I}_{B_2}^{B_2}\boldsymbol{\omega}^{B_1I}\right) = \mathbf{I}_{B_2}^{B_2}D^{B_2}\boldsymbol{\omega}^{B_2B} + \mathbf{I}_{B_2}^{B_2}D^B\boldsymbol{\omega}^{BI} + \left(\boldsymbol{\Omega}^{B_2B}\mathbf{I}_{B_2}^{B_2} + \boldsymbol{\Omega}^{BI}\mathbf{I}_{B_2}^{B_2} - \mathbf{I}_{B_2}^{B_2}\boldsymbol{\Omega}^{B_2B}\right)\boldsymbol{\omega}^{BI} + \left(\boldsymbol{\Omega}^{B_2B} + \boldsymbol{\Omega}^{BI}\right)\mathbf{I}_{B_2}^{B_2}\omega^{B_2B}. \tag{2.12}$$

The following conversion relations exist between the angular velocities:

$$\begin{aligned}\boldsymbol{\omega}^{B_2I} &= \boldsymbol{\omega}^{B_2B} + \boldsymbol{\omega}^{BI},\\ \boldsymbol{\omega}^{B_2B} &= \mathbf{0},\end{aligned} \tag{2.13}$$

where $\boldsymbol{\omega}^{B_2B} = \mathbf{0}$ because B_2 is fixed in the satellite body coordinate system.

Substituting (2.13) into (2.12) yields

$$D^I\left(\mathbf{I}_{B_2}^{B_2}\omega^{B_2I}\right) = \mathbf{I}_{B_2}^{B_2}D^B\boldsymbol{\omega}^{BI} + \boldsymbol{\Omega}^{BI}\mathbf{I}_{B_2}^{B_2}\boldsymbol{\omega}^{BI}. \tag{2.14}$$

For $D^I(m_{B_2}\mathbf{R}_{B_2B}D^I\mathbf{r}_{B_2B_1})$,

$$D^I\left(m_{B_2}\mathbf{R}_{B_2B}D^I\mathbf{r}_{B_2B_1}\right) = D^I\left(m_{B_2}\mathbf{r}_{B_2B} \times D^I\mathbf{r}_{B_2B_1}\right) = m_{B_2}D^I\mathbf{r}_{B_2B} \times D^I\mathbf{r}_{B_2B_1} + m_{B_2}\mathbf{R}_{B_2B}D^ID^I\mathbf{r}_{B_2B_1}, \tag{2.15}$$

where

$$\begin{aligned}D^I\mathbf{r}_{B_2B} \times D^I\mathbf{r}_{B_2B} &= 0,\\ D^I\mathbf{r}_{B_2B_1} &= \boldsymbol{\Omega}^{BI}\mathbf{r}_{B_2B_1} + D^B\mathbf{r}_{B_2B_1},\end{aligned} \tag{2.16}$$

$D^B\mathbf{r}_{B_2B_1} = \mathbf{0}$ because the position vector $\mathbf{r}_{B_2B_1}$ remains unchanged in the body coordinate system.

Substituting (2.16) into (2.15) yields

$$D^I\left(m_{B_2}\mathbf{R}_{B_2B}D^I\mathbf{r}_{B_1B}\right) = m_{B_2}\mathbf{R}_{B_2B}D^I\left(\boldsymbol{\Omega}^{BI}\mathbf{r}_{B_2B_1}\right). \tag{2.17}$$

Based on $D^I(s) = D^{B_1}(s) + \omega^{B_1I} \times s$, (2.17) becomes

$$m_{B_2}\mathbf{R}_{B_2B}D^I\left(\boldsymbol{\Omega}^{BI}\mathbf{r}_{B_2B_1}\right) = m_{B_2}\mathbf{R}_{B_2B}\boldsymbol{\Omega}^{BI}\boldsymbol{\Omega}^{BI}\mathbf{r}_{B_2B_1} + m_{B_2}\mathbf{R}_{B_2B}D^B\left(\boldsymbol{\Omega}^{BI}\mathbf{r}_{B_2B_1}\right). \tag{2.18}$$

Given that

$$D^B\left(\boldsymbol{\Omega}^{BI}\mathbf{r}_{B_2B_1}\right) = D^B\left(\boldsymbol{\omega}^{BI} \times \mathbf{r}_{B_2B_1}\right) = -D^B\left(\mathbf{r}_{B_2B_1} \times \boldsymbol{\omega}^{BI}\right) = -\mathbf{R}_{B_2B_1}D^B\boldsymbol{\omega}^{BI}, \tag{2.19}$$

then

$$D^I\left(m_{B_2}\mathbf{R}_{B_2B}D^I\mathbf{r}_{B_1B}\right) = m_{B_2}\mathbf{R}_{B_2B}\boldsymbol{\Omega}^{BI}\boldsymbol{\Omega}^{BI}\mathbf{r}_{B_2B_1} - m_{B_2}\mathbf{R}_{B_2B}\mathbf{R}_{B_2B_1}D^B\boldsymbol{\omega}^{BI}. \tag{2.20}$$

Based on (2.9), (2.11), (2.14), and (2.20), the attitude dynamic equation of a space-based observation satellite is as follows:

$$\begin{aligned}&\mathbf{I}_{B_1}^{B_1}D^{B_1}\boldsymbol{\omega}^{B_1B} + \mathbf{I}_{B_1}^{B_1}D^B\boldsymbol{\omega}^{BI} + \left(\boldsymbol{\Omega}^{B_1B}\mathbf{I}_{B_1}^{B_1} + \boldsymbol{\Omega}^{BI}\mathbf{I}_{B_1}^{B_1} - \mathbf{I}_{B_1}^{B_1}\boldsymbol{\Omega}^{B_1B}\right)\boldsymbol{\omega}^{BI} + \left(\boldsymbol{\Omega}^{B_1B} + \boldsymbol{\Omega}^{BI}\right)\mathbf{I}_{B_1}^{B_1}\boldsymbol{\omega}^{B_1B}\\ &\quad + \mathbf{I}_{B_2}^{B_2}D^B\boldsymbol{\omega}^{BI} + \boldsymbol{\Omega}^{BI}\mathbf{I}_{B_2}^{B_2}\boldsymbol{\omega}^{BI} + m_{B_2}\mathbf{R}_{B_2B}\boldsymbol{\Omega}^{BI}\boldsymbol{\Omega}^{BI}\mathbf{r}_{B_2B_1} - m_{B_2}\mathbf{R}_{B_2B}\mathbf{R}_{B_2B_1}D^B\boldsymbol{\omega}^{BI} = \mathbf{M}_B,\end{aligned} \tag{2.21}$$

where

$$\begin{aligned}\left[\mathbf{I}_{B_1}^{B_1}\right]^B &= [\mathbf{T}_{BB_1}]\left[\mathbf{I}_{B_1}^{B_1}\right]^{B_1}[\mathbf{T}_{BB_1}]^T,\\ \left[\boldsymbol{\Omega}^{B_1B}\right]^B &= [\mathbf{T}_{BB_1}]\left[\boldsymbol{\Omega}^{B_1B}\right]^{B_1}[\mathbf{T}_{BB_1}]^T,\\ \left[\boldsymbol{\omega}^{B_1B}\right]^B &= [\mathbf{T}_{BB_1}]\left[\boldsymbol{\omega}^{B_1B}\right]^{B_1}.\end{aligned} \tag{2.22}$$

Considering the orthogonality of $[\mathbf{T}_{BB_1}]$, the dynamic equation of attitude in the body coordinate system is as follows:

$$\begin{aligned}&[\mathbf{T}_{BB_1}]\left[\mathbf{I}_{B_1}^{B_1}\right]^{B_1}\left[D^{B_1}\boldsymbol{\omega}^{B_1B}\right]^{B_1} + [\mathbf{T}_{BB_1}]\left[\mathbf{I}_{B_1}^{B_1}\right]^{B_1}[\mathbf{T}_{BB_1}]^TD^B\boldsymbol{\omega}^{BI}\\ &\quad + \left([\mathbf{T}_{BB_1}]\left[\boldsymbol{\Omega}^{B_1B}\right]^{B_1}\left[\mathbf{I}_{B_1}^{B_1}\right]^{B_1}[\mathbf{T}_{BB_1}]^T + \boldsymbol{\Omega}^{BI}[\mathbf{T}_{BB_1}]\left[\mathbf{I}_{B_1}^{B_1}\right]^{B_1}[\mathbf{T}_{BB_1}]^T\right.\\ &\qquad \left.-[\mathbf{T}_{BB_1}]\left[\mathbf{I}_{B_1}^{B_1}\right]^{B_1}\left[\boldsymbol{\Omega}^{B_1B}\right]^{B_1}[\mathbf{T}_{BB_1}]^T\boldsymbol{\omega}^{BI}\right)\\ &\quad + \left([\mathbf{T}_{BB_1}]\left[\boldsymbol{\Omega}^{B_1B}\right]^{B_1}[\mathbf{T}_{BB_1}]^T + \left[\boldsymbol{\Omega}^{BI}\right]^B\right)[\mathbf{T}_{BB_1}]\left[\mathbf{I}_{B_1}^{B_1}\right]^{B_1}\left[\boldsymbol{\omega}^{B_1B}\right]^{B_1}\\ &\quad + \mathbf{I}_{B_2}^{B_2}D^B\boldsymbol{\omega}^{BI} + \boldsymbol{\Omega}^{BI}\mathbf{I}_{B_2}^{B_2}\boldsymbol{\omega}^{BI} + m_{B_2}\mathbf{R}_{B_2B}\boldsymbol{\Omega}^{BI}\boldsymbol{\Omega}^{BI}\mathbf{r}_{B_2B_1}\\ &\quad - m_{B_2}\mathbf{R}_{B_2B}\mathbf{R}_{B_2B_1}D^B\boldsymbol{\omega}^{BI} = \mathbf{M}_B.\end{aligned} \tag{2.23}$$

Assuming the disturbance torque introduced by the camera turntable is $\mathbf{M}_{\text{rotate}}$, then

$$\begin{aligned}\mathbf{M}_{\text{rotate}} = {} & [\mathbf{T}_{BB_1}]\left[\mathbf{I}_{B_1}^{B_1}\right]^{B_1}\left[D^{B_1}\boldsymbol{\omega}^{B_1B}\right]^{B_1} + [\mathbf{T}_{BB_1}]\left[\mathbf{I}_{B_1}^{B_1}\right]^{B_1}[\mathbf{T}_{BB_1}]^T D^B\boldsymbol{\omega}^{BI} \\ & + \Big([\mathbf{T}_{BB_1}]\left[\boldsymbol{\Omega}^{B_1B}\right]^{B_1}\left[\mathbf{I}_{B_1}^{B_1}\right]^{B_1}[\mathbf{T}_{BB_1}]^T + \boldsymbol{\Omega}^{BI}[\mathbf{T}_{BB_1}]\left[\mathbf{I}_{B_1}^{B_1}\right]^{B_1}[\mathbf{T}_{BB_1}]^T \\ & \quad -[\mathbf{T}_{BB_1}]\left[\mathbf{I}_{B_1}^{B_1}\right]^{B_1}\left[\boldsymbol{\Omega}^{B_1B}\right]^{B_1}[\mathbf{T}_{BB_1}]^T\Big)\boldsymbol{\omega}^{BI} \\ & + \Big([\mathbf{T}_{BB_1}]\left[\boldsymbol{\Omega}^{B_1B}\right]^{B_1}[\mathbf{T}_{BB_1}]^T + \left[\boldsymbol{\Omega}^{BI}\right]^{B}\Big)[\mathbf{T}_{BB_1}]\left[\mathbf{I}_{B_1}^{B_1}\right]^{B_1}\left[\boldsymbol{\omega}^{B_1B}\right]^{B_1}.\end{aligned} \tag{2.24}$$

The satellite attitude dynamic equation can then be simplified as

$$\mathbf{I}_{B_2}^{B_2}D^B\boldsymbol{\omega}^{BI} + \boldsymbol{\Omega}^{BI}\mathbf{I}_{B_2}^{B_2}\boldsymbol{\omega}^{BI} + \mathbf{M}_{\text{rotate}} = \mathbf{M}_B. \tag{2.25}$$

2.2.2. Dynamic Model of a Space-Based Observation Satellite with Reaction Wheels

The reaction wheel, as the actuator of a satellite, is used to adjust the satellite attitude. When equipped with reaction wheels, the total moment of momentum of a satellite becomes

$$D^I\mathbf{L}_B^{BI} = D^I\left(\mathbf{L}_B^{B_1I} + \mathbf{L}_B^{B_2I} + \mathbf{L}_B^{WB}\right) = D^I\left(\mathbf{L}_B^{B_1I} + \mathbf{L}_B^{B_2I}\right) + D^B\mathbf{L}_B^{WB} + \boldsymbol{\Omega}^{BI}\mathbf{L}_B^{WB}. \tag{2.26}$$

From (2.25) and (2.26), the attitude dynamic equation of a space-based observation satellite with reaction wheels is as follows:

$$\mathbf{I}_{B_2}^{B_2}D^B\boldsymbol{\omega}^{BI} + \boldsymbol{\Omega}^{BI}\mathbf{I}_{B_2}^{B_2}\boldsymbol{\omega}^{BI} + \boldsymbol{\Omega}^{BI}\mathbf{L}_B^{WB} + \mathbf{M}_{\text{rotate}} = \mathbf{M}_B + \mathbf{M}_f, \tag{2.27}$$

where $\mathbf{M}_f = -D^B\mathbf{L}_B^{WB}$ is the control torque produced by a reaction wheel.

2.2.3. Dynamic Model of a Space-Based Observation Satellite with Flexible Appendages

The motion equation of solar panels is [6]

$$\ddot{\mathbf{q}} + 2\boldsymbol{\xi}\dot{\mathbf{q}} + \boldsymbol{\Lambda}^2\mathbf{q} + \mathbf{C}^T\dot{\boldsymbol{\omega}} = 0, \tag{2.28}$$

where $\mathbf{q}$ is the flexible modal coordinates, $\mathbf{C}^T$ is the coupling matrix between the solar panel and satellite body, $\boldsymbol{\xi}$ is the structural damping of the solar panel, and $\boldsymbol{\Lambda}$ is the vibration frequency of the solar panel.

Then, the attitude dynamic model of the satellite with a reaction wheel and flexible appendages is

$$\mathbf{I}_{B_2}^{B_2}D^B\boldsymbol{\omega}^{BI} + \boldsymbol{\Omega}^{BI}\mathbf{I}_{B_2}^{B_2}\boldsymbol{\omega}^{BI} + \boldsymbol{\Omega}^{BI}\mathbf{L}_B^{WB} + \mathbf{C}\ddot{\mathbf{q}} + \mathrm{M}_{\text{rotate}} = \mathbf{M}_B + \mathbf{M}_f. \tag{2.29}$$

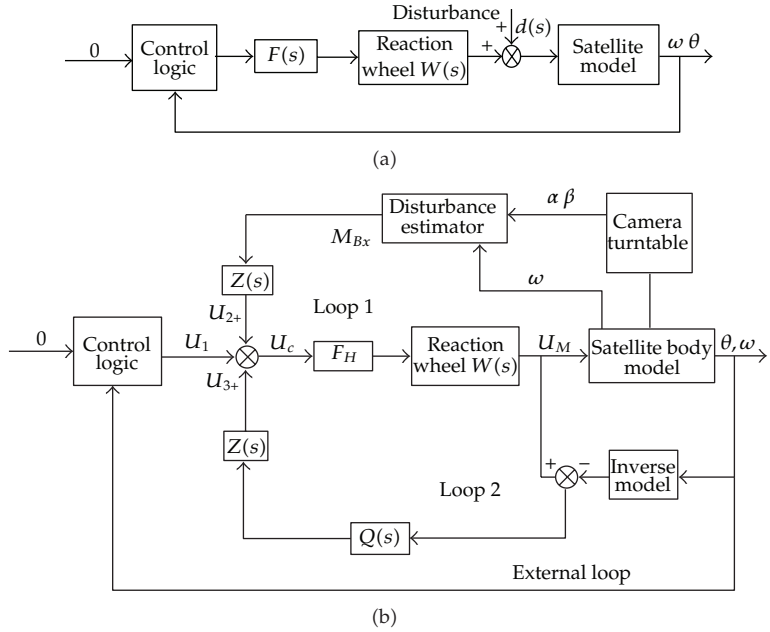

Figure 4: Structure of the attitude control system. (a) The conventional method used in Japanese HALCA satellite. (b) The method proposed in this paper.

3. Dual-Loop Compensation-Based High-Precision Attitude Control

A matter of primary concern in designing high-accuracy attitude control is how to eliminate the disturbance introduced by rotation of rigid parts and flexible solar panels. [6] have applied the attitude control system as shown in Figure 4(a) to the Japanese satellite HALCA for the very long baseline interferometry observations in orbit. $F(s)$ is a third-order low-pass filter, called the Chebyshev-type filter. Therefore,

$$F(s) = \frac{1}{0.686s^3 + 0.736s^2 + 2.061\tau s + 1}, \tag{3.1}$$

where the cut-off frequency of $F(s)$ is 0.286 Hz.

In this paper, a novel dual-loop DOB is proposed as shown in Figure 4(b), where the DOB includes two parts: loop 1 is used to compensate for the disturbance introduced by the motion of the turntable, while loop 2 is used to compensate for the disturbance made by solar panels. The numerical simulation results show that the proposed method is far superior to the conventional method.

3.1. Design of Loop 1

Based on (2.24), the estimation of disturbance introduced by the turntable is as follows:

$$\begin{aligned}\widehat{\mathbf{M}}_{\text{rotate}} = {} & [\mathbf{T}_{BB_1}]\left[\mathbf{I}_{B_1}^{B_1}\right]^{B_1}\left[D^{B_1}\boldsymbol{\omega}^{B_1B}\right]^{B_1} + [\mathbf{T}_{BB_1}]\left[\mathbf{I}_{B_1}^{B_1}\right]^{B_1}[\mathbf{T}_{BB_1}]^T D^B\boldsymbol{\omega}^{BI} \\ & + \left(\boldsymbol{\Omega}^{BI}[\mathbf{T}_{BB_1}]\left[\mathbf{I}_{B_1}^{B_1}\right]^{B_1}[\mathbf{T}_{BB_1}]^T\right)\boldsymbol{\omega}^{BI} + [\mathbf{T}_{BB_1}]\left[\boldsymbol{\Omega}^{B_1B}\right]^{B_1}\left[\mathbf{I}_{B_1}^{B_1}\right]^{B_1}\left[\boldsymbol{\omega}^{B_1B}\right]^{B_1} \\ & + m_{B_2}\mathbf{R}_{B_2B}\boldsymbol{\Omega}^{BI}\boldsymbol{\Omega}^{BI}\mathbf{r}_{B_2B_1} - m_{B_2}\mathbf{R}_{B_2B}\mathbf{R}_{B_2B_1}D^B\boldsymbol{\omega}^{BI} \\ & + \left(\left[\mathbf{T}^{BB_1}\right]\left[\boldsymbol{\Omega}^{B_1B}\right]^{B_1}\left[\mathbf{I}_{B_1}^{B_1}\right]^{B_1}\left[\mathbf{T}^{BB_1}\right]^T - \left[\mathbf{T}^{BB_1}\right]\left[\mathbf{I}_{B_1}^{B_1}\right]^{B_1}\left[\boldsymbol{\Omega}^{B_1B}\right]^{B_1}\left[\mathbf{T}^{BB_1}\right]^T\right)\boldsymbol{\omega}^{BI} \\ & + \left[\boldsymbol{\Omega}^{BI}\right]^B\left[\mathbf{T}^{BB_1}\right]\left[\mathbf{I}_{B_1}^{B_1}\right]^{B_1}\left[\boldsymbol{\omega}^{B_1B}\right]^{B_1}, \end{aligned} \tag{3.2}$$

$$\widehat{\mathbf{M}}_{\text{rotate}} = \begin{bmatrix}\widehat{M}_{Bx}\\ \widehat{M}_{By}\\ \widehat{M}_{Bz}\end{bmatrix}.$$

Then the estimation of disturbance in x-axis is

$$\begin{aligned}\widehat{M}_{Bx} = {} & I_{B_1x}\left(\dot{\omega}_{x1}\mathrm{c}\beta + \dot{\omega}_{y1}\mathrm{s}\alpha\mathrm{s}\beta + \dot{\omega}_{z1}\mathrm{c}\alpha\mathrm{s}\beta + \dot{\omega}_x + \omega_y\omega_{z1}\mathrm{c}\alpha\mathrm{c}\beta - \omega_y\omega_{x1}\mathrm{s}\beta\right. \\ & \left.+\omega_y\omega_{y1}\mathrm{s}\alpha\mathrm{c}\beta - \omega_z\omega_{y1}\mathrm{c}\alpha + \omega_z\omega_{z1}\mathrm{s}\alpha\right) \\ & + I_{B_1y}\Big(-\omega_y\omega_{z1}\mathrm{c}\alpha\mathrm{c}\beta + \omega_y\omega_{x1}\mathrm{s}\beta - \omega_y\omega_{y1}\mathrm{s}\alpha\mathrm{c}\beta - \omega_y\omega_z \\ & - \omega_{y1}\omega_{z1}\mathrm{c}^2\alpha\mathrm{c}\beta + \omega_{x1}\omega_{y1}\mathrm{c}\alpha\mathrm{s}\beta - \omega_{y1}^2\mathrm{s}\alpha\mathrm{c}\alpha\mathrm{c}\beta + \omega_{z1}^2\mathrm{s}\alpha\mathrm{c}\alpha\mathrm{c}\beta \\ & -\omega_{x1}\omega_{z1}\mathrm{s}\alpha\mathrm{s}\beta + \omega_{y1}\omega_z\mathrm{s}^2\alpha\mathrm{c}\beta - \omega_z\omega_{y1}\mathrm{c}\alpha + \omega_z\omega_{z1}\mathrm{s}\alpha\Big) \\ & + I_{B_1z}\left(\omega_z\omega_{y1}\mathrm{c}\alpha - \omega_z\omega_{z1}\mathrm{s}\alpha + \omega_y\omega_z - \omega_{x1}\omega_{y1}\mathrm{c}\alpha\mathrm{s}\beta + \omega_{x1}\omega_{z1}\mathrm{s}\alpha\mathrm{s}\beta\right. \\ & + \omega_{y1}^2\mathrm{s}\alpha\mathrm{c}\alpha\mathrm{c}\beta - \omega_{y1}\omega_{z1}\mathrm{s}^2\alpha\mathrm{c}\beta + \omega_{y1}\omega_{z1}\mathrm{c}^2\alpha\mathrm{c}\beta - \omega_{z1}^2\mathrm{s}\alpha\mathrm{c}\alpha\mathrm{c}\beta \\ & \left.-\omega_y\omega_{x1}\mathrm{s}\beta + \omega_y\omega_{y1}\mathrm{s}\alpha\mathrm{c}\beta + \omega_y\omega_{z1}\mathrm{c}\alpha\mathrm{c}\beta\right) + I_{B_2x}\dot{\omega}_x - \omega_y\omega_z I_{B_2y} + \omega_y\omega_z I_{B_2z}, \end{aligned} \tag{3.3}$$

where α, β, ω_x, ω_y, and ω_z can be measured by sensors on the satellite. ω_{x1}, ω_{y1}, and ω_{z1} can be yielded by (2.4).

The model of the reaction wheel is described as

$$A(s) = \frac{K_m}{T_m s + 1}s. \tag{3.4}$$

Therefore, $Z(s)$ is given by

$$Z(s) = \frac{T_m s + 1}{K_m s}. \tag{3.5}$$

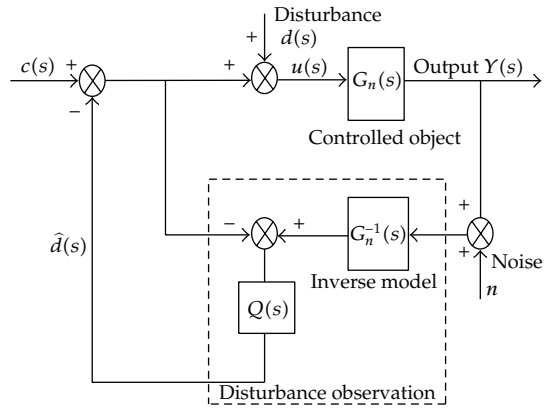

Figure 5: Block diagram of the disturbance observer.

The compensation of loop1 in x-axis is then described as

$$U_2 = Z(s)M_{Bx}. \tag{3.6}$$

3.2. Design of Loop 2

A description of the basic structure of disturbance observer is shown in Figure 5. The system output can be expressed in terms of the reference control input, the external disturbance, and the measurement noise. Thus, the behavior of the actual system is to be the same as the given nominal model.

From Figure 5 we can find

$$u(s) = c(s) - \hat{d}(s) + d(s), \tag{3.7}$$

where $c(s)$ is the controller output and $\hat{d}(s)$ is the disturbance estimation.

And we can also find

$$\begin{aligned} G_{CY}(s) &= \frac{Y(s)}{U(s)} = \frac{G_p(s)G_n(s)}{G_n(s) + Q(s)\left(G_p(s) - G_n(s)\right)}, \\ G_{DY}(s) &= \frac{Y(s)}{D(s)} = \frac{G_p(s)G_n(s)(1 - Q(s))}{G_n(s) + Q(s)\left(G_p(s) - G_n(s)\right)}, \\ G_{NY}(s) &= \frac{Y(s)}{N(s)} = \frac{G_p(s)Q(s)}{G_n(s) + Q(s)\left(G_p(s) - G_n(s)\right)}. \end{aligned} \tag{3.8}$$

Assuming f_q is the cut-off frequency of low-pass filter $Q(s)$ and f is the signal frequency. When $f \leq f_q$, $Q \approx 1$, $G_{CY}(s) \approx G_n(s)$, $G_{DY} \approx 0$, $G_{NY} \approx 1$.

This shows that in low-frequency range the disturbance observer could make system characteristics approximately equal to the nominal model characteristics, and the disturbance observer can overcome the various disturbances effectively.

In this section, the nonlinear terms and small quantities in the satellite dynamics are treated as the external disturbances so that linear controller design tools (Laplace transform, disturbance observer) can be utilized. We take the x-axes as examples to design loop 2. Taking the $\mathbf{\Omega}^{BI}\mathbf{L}_B^{WB}, \mathbf{C\ddot{q}}, \mathbf{M}_{\text{rotate}}$ in the satellite dynamics equation (2.29) as external disturbances, then the x-axis nominal modal could be written as

$$G_n(s) = \frac{1}{I_x\omega_x s + (I_z - I_y)\omega_z\omega_y}. \tag{3.9}$$

Then the inverse model is

$$G_n{}^{-1}(s) = I_x\omega_x s + (I_z - I_y)\omega_z\omega_y. \tag{3.10}$$

The $Q(s)$ is a key part in loop 2, which has the form [11]:

$$Q(s) = \left[1 + \sum_{k=1}^{N-r} a_k(\tau s)^k\right]\left[1 + \sum_{k=1}^{N} a_k(\tau s)^k\right]^{-1}, \tag{3.11}$$

where N is the order of $Q(s)$, τ is the filter time constant, and r is the relative degree of $Q(s)$.

The main issue in the design of $Q(s)$ is the tradeoff between making $|Q(jw)|$ small and $|1 - Q(jw)|$ small [12]. One of the typical solutions is to choose $Q(s)$ so that the right-hand-side slope of $|Q(jw)|$ is the same as the left-hand-side slope of $|1 - Q(jw)|$. In the frequency domain, the slope of $|Q(jw)|$ in low frequency and the slope of $|1 - Q(jw)|$ in high frequency are, respectively, approximated as [12]

$$\begin{aligned} \frac{\text{Lm}|1 - Q(jw)|}{\text{Lm}(w)} &\approx N - r + 1, \\ \frac{\text{Lm}|Q(jw)|}{\text{Lm}(w)} &\approx -r, \end{aligned} \tag{3.12}$$

where Lm is log magnitude. Since the optimal $Q(s)$ is obtained by letting the slopes be equivalent, the following relation is achieved:

$$r = \frac{(N+1)}{2}. \tag{3.13}$$

It is notable that the Q_{31}-filter is obtained as the minimum-order Q-filter for the second-order system [12]

$$Q_{31}(s) = \frac{3\tau s + 1}{s^3 + 3\tau s^2 + 3\tau s + 1}, \tag{3.14}$$

where τ is the time constant.

The compensation of loop 2 as shown in Figure 4(b) in x-axis is then described as

$$U_3 = Z(s)Q(s)\left[U_M - I_x\omega_x s - \left(I_z - I_y\right)\omega_y\omega_z\right]. \tag{3.15}$$

Other axes employ the same compensation structure as (3.15).

3.3. Design of the External Loop

There are many uncertain factors in the parameters and structure of an observation satellite. For example, the moment of inertia J of the system is not quite accurate, and the space environmental disturbance torques, such as gravity gradient torque, aerodynamic torque and, solar radiation torque, are uncertainties. For a satellite in 1000 km orbit, a typical environmental disturbance torque equation is written as

$$\begin{aligned} M_x &= 10^{-5}(3\cos\omega_0 t + 1), \\ M_y &= 10^{-5}(1.5\ \sin\omega_0 t + 3\cos\omega_0 t), \\ M_z &= 10^{-5}(3\sin\omega_0 t + 1). \end{aligned} \tag{3.16}$$

Consequently, the control scheme must robustly restrain all uncertainties, and the property of the actuators must be considered. The control law should be suitable for limited and discontinuous control torque and gas consumption.

The SMC method has some advantages, such as robustness to parameter uncertainty, insensitivity to bounded disturbances, fast dynamic response, a remarkable computational simplicity with respect to other robust control approaches, and easy implementation of the controller.

Variable structure control (VSC) is recognized as a powerful theoretical technique for robust control, even under variations in system parameters or in the presence of external disturbances. A well-known property of a VSC system is that its sliding modes are invariant with respect to a class of disturbances and parameter perturbations. If the disturbances and perturbations are bounded, the so-called reaching process is also robust against them with the controller appropriately designed. Thus, in this paper, VSC was employed as the external loop controller, which is written as

$$\mathbf{U} = \begin{cases} -T \cdot \operatorname{sgn}(s) & |s| > \delta_1 \\ -T_f \cdot \operatorname{sgn}(s) & \delta < |s| < \delta_1 \\ -T_f \cdot \dfrac{s}{\delta} & |s| < \delta, \end{cases} \tag{3.17}$$

$$s = ce + \dot{e},$$

where s is the sliding mode, δ_1 is a bound value for adjusting the thrusters and wheels, δ is the cutting gene to avoid vibrations of the VSC on the switching surface, T_p is the thruster maximal output torque, T_f is the wheel maximal output torque, e is the angle error (Figure 6), and $\dot{e}$ is the angular velocity error.

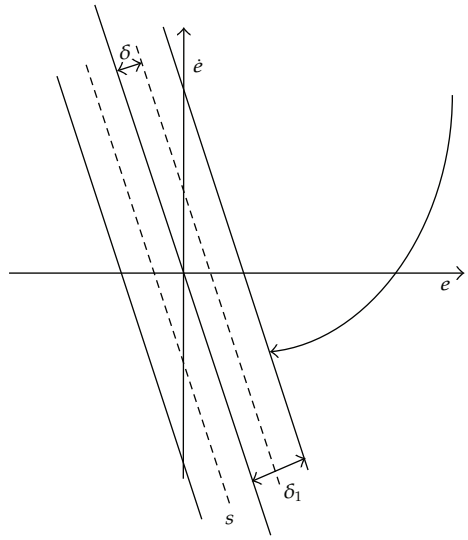

Figure 6: Track of the system in the phase plane.

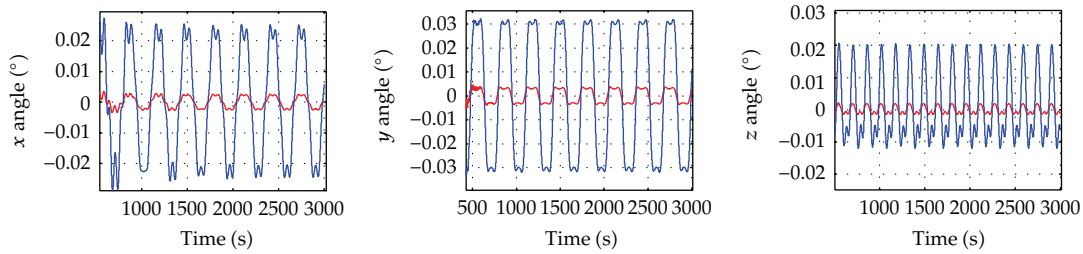

Figure 7: Angle error results: (a) x-, (b) y-, and (c) z-axes. The red line represents proposed method. The blue line represents conventional method.

Considering the effects produced by the motion of the two-dimensional turntable and elastic vibration of flexible panels, the disturbance estimation can be used as the forward to compensate for the disturbance from the camera turntable.

Then, the final control law is rewritten as follows:

$$\mathbf{U} = \begin{cases} -T \cdot \operatorname{sgn}(s) & |s| > \delta_1 \\ -T_f \cdot \operatorname{sgn}(s) & \delta < |s| < \delta_1 \\ -\dfrac{T_f \cdot s}{\delta + \mathbf{U_2} + \mathbf{U_3}} & |s| < \delta, \end{cases} \tag{3.18}$$

where $\mathbf{U}_2$, $\mathbf{U}_3$ are the compensations of disturbance by the DOB.

Filter $F_H(s)$ is to prevent excitation of the ignored higher flexible-mode's vibration, where we chose a common filter structure as

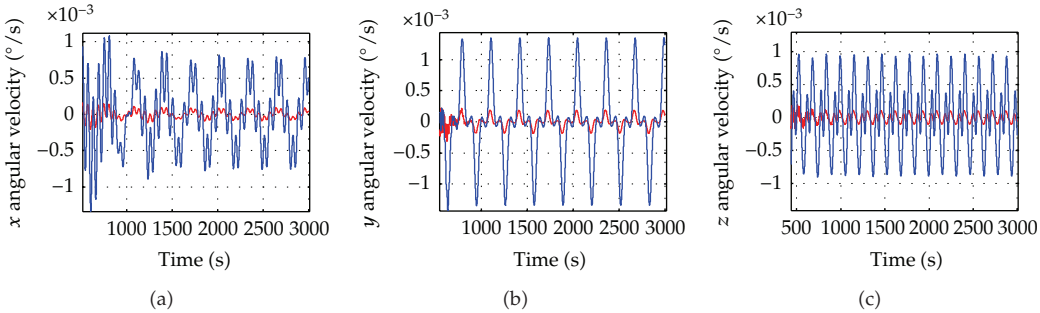

Figure 8: Angular velocity error results: (a) x-, (b) y-, and (c) z-axes. The red line represents proposed method. The blue line represents conventional method.

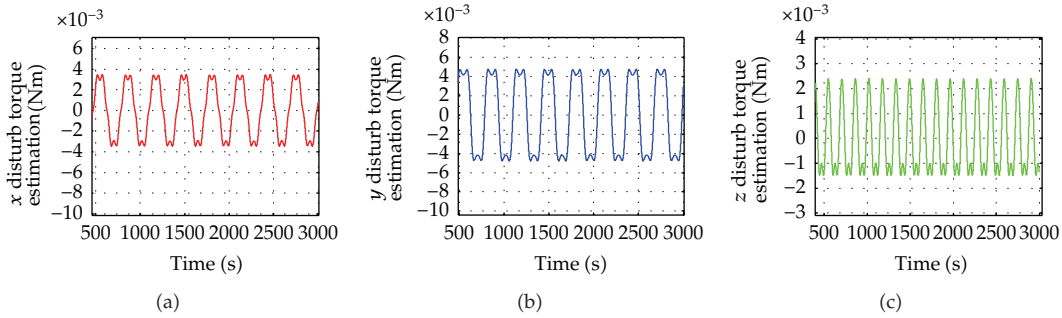

Figure 9: Estimation of the disturbance torques.

$$F_H = \frac{\omega_h}{s + \omega_h}, \tag{3.19}$$

where ω_h is the cut-off frequency. It is preferred that the cut-off frequency ω_h of F_H is designed equal to or lower than the bandwidth of the $Q(s)$. In this paper, the cut-off frequency of $Q(s)$ is 0.6, so ω_h is set as 0.6.

4. Numerical Simulation and Results

In this section, the results and analysis from the algorithm developed to control the space-based observation micro-satellite are presented. For some space observation tasks, the objective of the control system is to keep the satellite attitude angle error $< 0.02°$ and the angular velocity error $< 0.001°/s$.

4.1. Initial Assumptions

See Tables 1 and 2.

Table 1

Initial parameters of satellite	Value
Initial attitude angle of satellite	$\theta_x = 1^\circ,\ \theta_y = 1^\circ,\ \theta_z = 1^\circ$
Initial attitude angular velocity of satellite	$\omega_x = 0.1^\circ/s,\ \omega_y = 0.1^\circ/s,\ \omega_z = 0.1^\circ/s$
Angular velocity of camera turntable	$\alpha = (1.2\sin\omega t)^\circ/s, \beta = (1.2\sin\omega t)^\circ/s$
	$\omega = 0.03\,\mathrm{rad}/s$
The uncertainties of the matrix of moment of inertia	$\Delta I = \begin{bmatrix} 3 & 0 & 0 \\ 0 & 4 & 0 \\ 0 & 0 & 2 \end{bmatrix} (\mathrm{kg}\cdot\mathrm{m}^2)$
Space environmental disturbance torques	$M_x = 10^{-5}(3\cos\omega_0 t + 1)$ $M_y = 10^{-5}(1.5\sin\omega_0 t + 3\cos\omega_0 t)$ $M_z = 10^{-5}(3\sin\omega_0 t + 1)$

Table 2: Satellite parameters.

Satellite parameters	Value
Mass of platform m_2	$m_2 = 250\,\mathrm{kg}$
Mass of camera turntable m_1	$m_1 = 30\,\mathrm{kg}$
The matrix of moment of inertia of platform I_{B_2}	$I_{B_2} = \begin{bmatrix} 90 & 0 & 0 \\ 0 & 150 & 0 \\ 0 & 0 & 85 \end{bmatrix} (\mathrm{kg}\cdot\mathrm{m}^2)$
The matrix of moment of inertia of camera turntable I_{B_1}	$I_{B_1} = \begin{bmatrix} 9 & 0 & 0 \\ 0 & 15 & 0 \\ 0 & 0 & 8.5 \end{bmatrix} (\mathrm{kg}\cdot\mathrm{m}^2)$
$r_{B_2B_1}$	$\lvert r_{B_2B_1}\rvert = 0.8\,\mathrm{m}$
r_{B_2B}	$\lvert r_{B_2B}\rvert = 0.08\,\mathrm{m}$
Maximal output torque of reaction wheel	$0.1\,\mathrm{Nm}$
The matrix coupling coefficient of solar panel	$C = \begin{bmatrix} -2.8137 & 0 & 0 \\ 0 & 3.142 & 0 \\ -0.0441 & 0 & 1.826 \end{bmatrix}$
Vibration frequency of solar panels Λ	$\Lambda = \begin{bmatrix} 0.11 & 0 & 0 \\ 0 & 0.33 & 0 \\ 0 & 0 & 0.73 \end{bmatrix} \mathrm{Hz}$
Structural damping of solar panels	$\xi = 0.002$

Table 3: Comparison of the results of the two cases.

	Angle errors	Angular velocity errors
The conventional method	0.03°	$\left(1.2\times10^{-3}\right)^\circ/\mathrm{s}$
The proposed method	0.004°	$\left(0.2\times10^{-3}\right)^\circ/\mathrm{s}$

4.2. Results

See Figures 7, 8, and 9, and Table 3.

4.3. Conclusion

From Figures 7–9 and Table 3, we can conclude that by the dual-loop DOB, the control method proposed in this paper can significantly reduce the errors of attitude angle and angular velocity (as shown in Table 3), and the proposed control scheme can meet the requirements of the attitude control task. In addition, the derived-dynamic model of a space-based observation satellite has a high reference value to the design of attitude control systems for space-based observation satellites.

Nomenclature

B:	Centroid of satellite
B_1:	Centroid of payload
B_2:	Centroid of platform
m_{B1}:	Mass of payload
m_{B2}:	Mass of platform
$\mathbf{r}_{B_2B}$:	Distance vector from B to B_2, $\mathbf{R}_{B_2B}$ is its antisymmetric matrix
$\mathbf{r}_{B_1B}$:	Distance vector from B to B_1, $\mathbf{R}_{B_1B}$ is its antisymmetric matrix
$\boldsymbol{\omega}^{BI}$:	Angular velocity vector of the satellite body frame relative to the inertial frame
$\boldsymbol{\Omega}^{BI}$:	Is its antisymmetric matrix
$\boldsymbol{\omega}^{B_1B}$:	Angular velocity vector of the camera frame relative to the satellite body frame
$\boldsymbol{\Omega}^{B_1B}$:	Is its antisymmetric matrix
$D^I = (d/dt)\|_I$:	Differential in the inertial frame
$D^B = (d/dt)\|_B$:	Differential in the satellite body frame
$D^{B_1} = (d/dt)\|_{B_1}$:	Differential in the camera frame
$\mathbf{I}_C^{CI}$:	Inertia matrix of rigid body C relative to point C
$\mathbf{L}_B^{B_1I}$:	Moment of momentum of the camera turntable relative to B in the inertial frame
$\mathbf{L}_B^{B_2I}$:	Moment of momentum of the platform relativeto B in the inertial frame
$\mathbf{L}_B^{WB}$:	Moment of momentum of the reaction wheel
$\mathbf{T}_{BI}$:	Transformation matrix from the inertial frame to the satellite body frame
$\mathbf{T}_{B_1B}$:	Transformation matrix from the satellite body frame to the payload frame
sα:	$\sin\alpha$
cα :	$\cos\alpha$
sβ :	$\sin\beta$
cβ :	$\cos\beta$.

Acknowledgments

This paper was funded by the National Natural Science Foundation of China no. 60904089 and the Fundamental Research Funds for the Central Universities of China.

References

[1] L. Cheng, T. Wang, and J. Li, "Attitude dynamics and control of a flexible multi-body satellite," *Journal of Tsinghua University*, vol. 45, no. 11, pp. 1506–1509, 2005.

[2] G. Li, J. Zhou, and F. Zhou, "Intelligent control research of multibody satellite for high stability," *Chinese Space Science and Technology*, vol. 27, no. 2, pp. 151–156, 2007.

[3] B. S. Chen, C. S. Wu, and Y. W. Jan, "Adaptive fuzzy mixed H_2/H_∞ attitude control of spacecraft," *IEEE Transactions on Aerospace and Electronic Systems*, vol. 36, no. 4, pp. 1343–1359, 2000.

[4] M. Azadi, S. A. Fazelzadeh, M. Eghtesad, and E. Azadi, "Vibration suppression and adaptive-robust control of a smart flexible satellite with three axes maneuvering," *Acta Astronautica*, vol. 69, no. 5-6, pp. 307–322, 2011.

[5] Y. W. Jan and J. C. Chiou, "Minimum-time spacecraft maneuver using sliding-mode control," *Acta Astronautica*, vol. 54, no. 1, pp. 69–75, 2003.

[6] T. Yamashita, N. Ogura, T. Kurii, and T. Hashimoto, "Improved satellite attitude control using a disturbance compensator," *Acta Astronautica*, vol. 55, no. 1, pp. 15–25, 2004.

[7] M. De La Sen and N. Luo, "Design of linear observers for a class of linear hybrid systems," *International Journal of Systems Science*, vol. 31, no. 9, pp. 1077–1090, 2000.

[8] M. De la Sen, A. Ibeas, and S. Alonso-Quesada, "Observer-based vaccination strategy for a true mass action SEIR epidemic model with potential estimation of all the populations," *Discrete Dynamics in Nature and Society*, vol. 2011, Article ID 743067, 19 pages, 2011.

[9] M. Santhakumar, "Proportional-derivative observer-based backstepping control for an underwater manipulator," *Mathematical Problems in Engineering*, vol. 2011, Article ID 397092, 18 pages, 2011.

[10] C. J. Kempf and S. Kobayashi, "Disturbance observer and feedforward design for a high-speed direct-drive positioning table," *IEEE Transactions on Control Systems Technology*, vol. 7, no. 5, pp. 513–526, 1999.

[11] B. Yao, M. Al-Majed, and M. Tomizuka, "High-performance robust motion control of machine tools: an adaptive robust control approach and comparative experiments," *IEEE/ASME Transactions on Mechatronics*, vol. 2, no. 2, pp. 63–76, 1997.

[12] B. K. Kim and W. K. Chung, "Advanced disturbance observer design for mechanical positioning systems," *IEEE Transactions on Industrial Electronics*, vol. 50, no. 6, pp. 1207–1216, 2003.